Husky 2011 walkaway 3C-VSP

Kevin W. Hall, Don C. Lawton, Dawson Holloway, and Eric V. Gallant

ABSTRACT

CREWES was a participant in a walk-away vertical seismic profile (VSP) test near Cold Lake. Two-hundred and twenty-two VectorSeis accelerometers were deployed in a well at a nominal two meter spacing. Fourteen source points were acquired with dynamite and the University of Calgary's EnviroVibe source without moving the string of accelerometers in the well. P-S wavefields are observed on the radial and transverse components, and S-S wavefields are visible on the vertical, radial and transverse components for most shots. Higher amplitude down-going S-waves were generated from the vibrator source compared to dynamite. Three methods to perform automated component rotation are tested, and shown to give similar results, which are consistent between both source types. P-P and P-S brute corridor stacks are produced and compared to synthetic seismograms.

INTRODUCTION

The University of Calgary EnviroVibe was used as a source for a walk-away vertical seismic profile (VSP) near Cold Lake, Alberta, in a field that is being actively produced by steam assisted gravity drainage (SAGD). Two-hundred and twenty-two VectorSeis accelerometers were deployed in a dry well at a nominal two meter spacing. The accelerometers were magnetically clamped to the inside of steel casing. The large number of receivers in the borehole allowed acquisition to proceed without moving the receiver array in the well.

Source point locations relative the borehole are shown in Figure 1. Source point elevations, offsets and azimuths relative to the well are detailed in Figure 2. Fourteen source points were acquired twice, once with 0.125 kg of dynamite at 9 m depth, and once with the EnviroVibe running a 10-300 Hz linear sweep over 20 s (Table 1). Source point 1 was closest to the well at 12 m offset, and source point 14 was the furthest away at 1031 m. (Figures 1 and 2). All data were acquired at night, with surface temperatures in the -5 to -10 degree Celsius range. There was no wind at time of acquisition.

The EnviroVibe sweep had some phase distortions at high frequencies in the field during this survey. It was found that a long taper at the high end of the sweep enabled acquisition of at least some of the desired high frequencies, and this was done instead of terminating the sweep at something slightly less than 300 Hz. Acquisition parameters are summarized in Table 1.

This report provides an initial evaluation of the datasets acquired during the survey, and outlines directions for future work.

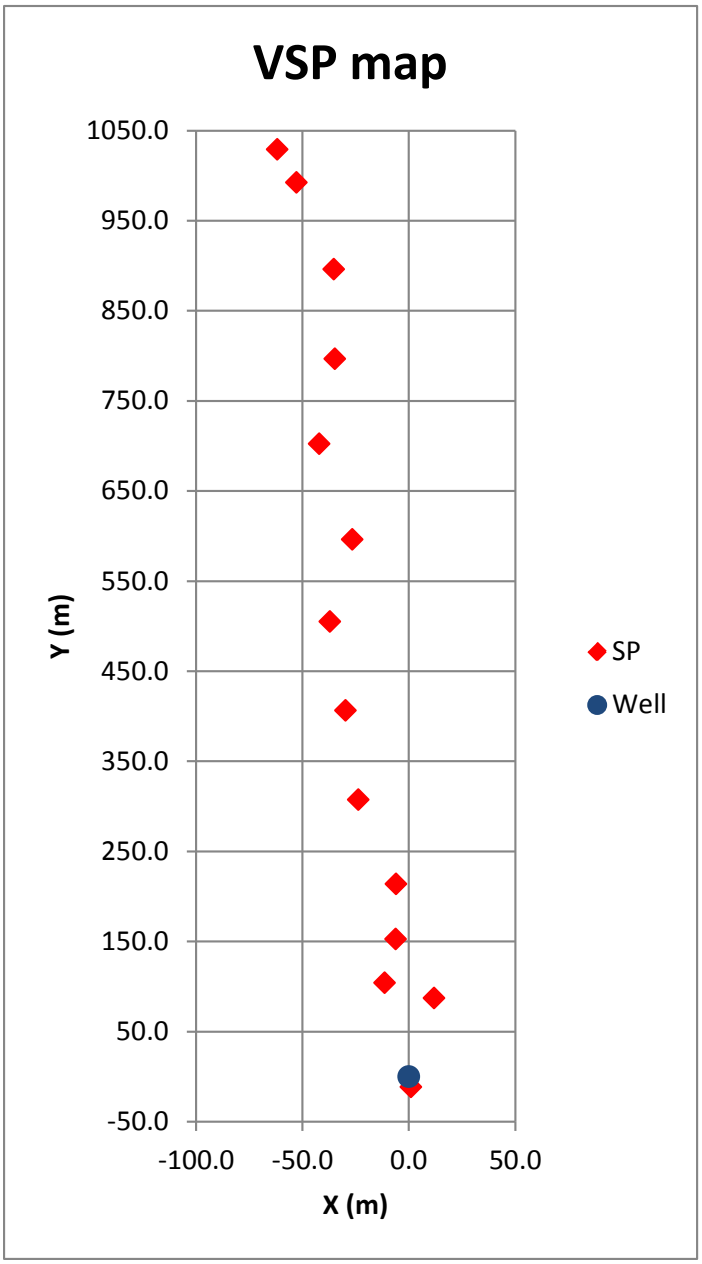

FIG. 1. Map showing source point locations relative to the well location. Well location is plotted at co-ordinates (0,0).

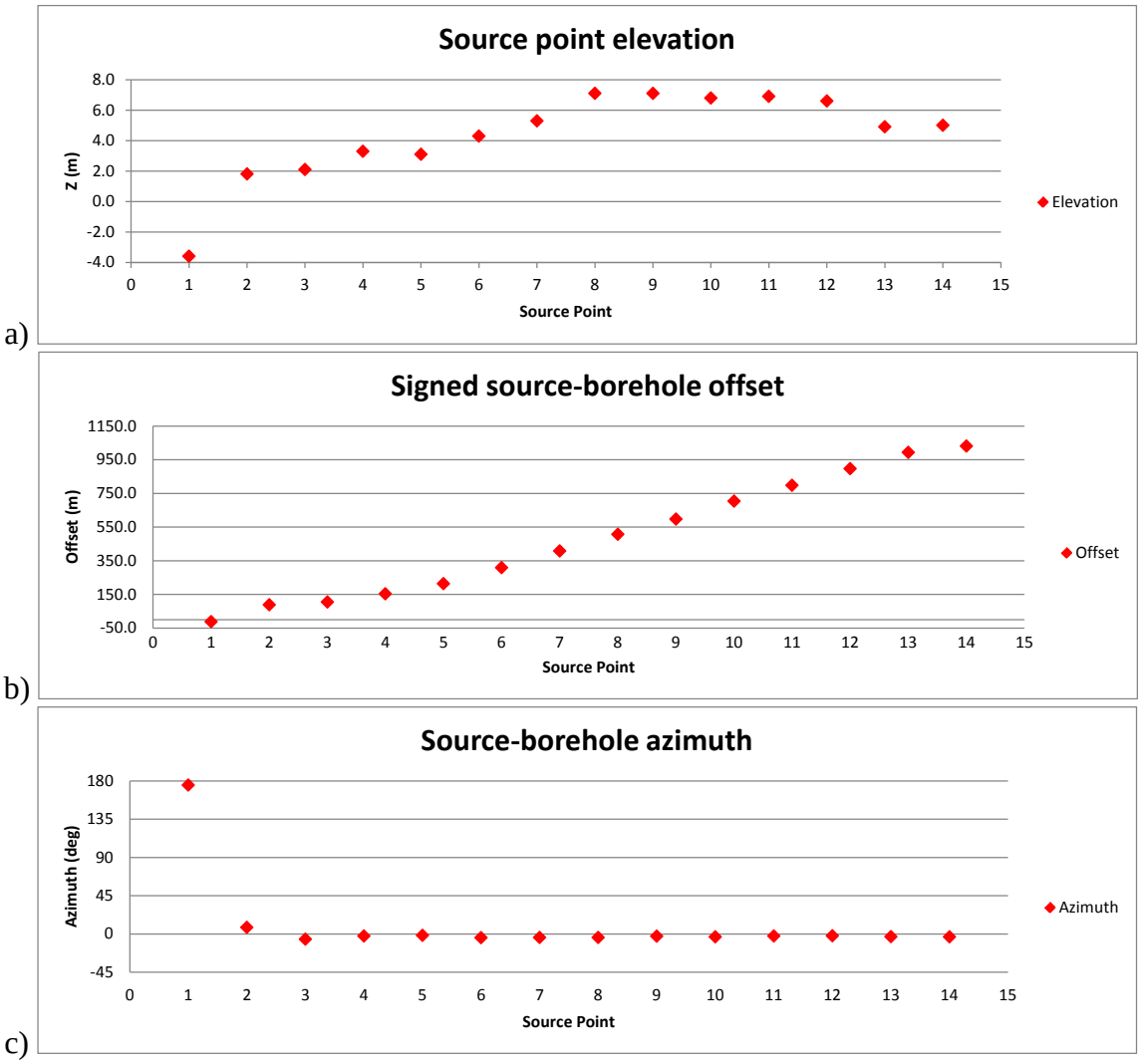

FIG. 2. Source point elevation relative to well ground elevation (a), distance from well (b), and azimuth of source point from the well, relative to grid north (c).

Table 1. Acquisition parameters.

Dynamite	0.125kg	9 m depth	
Vibroseis	10-300 Hz over 20 s	Linear. One sweep per vibe point.	100 ms start taper, 1000 ms end taper
Receivers	VectorSeis	222 X3C sensors at nominal 2 m spacing. Depth range 60 – 500 m	Magnetically attached to inside of steel casing.
Borehole	562 m TD	Vertical	No fluids in borehole
Record	1 ms sample rate	3 s trace length	

Horizontal component rotation

While the vertical component can be assumed to be vertical, the horizontal channels have an unknown orientation in the borehole. It is possible for each receiver to be clamped to the casing in a different orientation than its neighbors, and it is also possible for the string to spiral down the inside of the casing on insertion. After receiving copies of the field data, CREWES performed automated component rotations using the ProMAX module, '3-Component Rcvr Orientation.' This module has three choices for the method used for component rotation, namely peak vector amplitude, principal component analysis of Eigen vectors of hodograms, and maximum power search. While the module will perform three-component rotations, we chose at this stage to apply two-component rotations to the horizontal channels only, using data from a 60 ms window centred on the vertical component first-break picks.

The ProMAX module outputs trace headers ORIG_AZM, ORIG_INCL, COM_AZIM, COM_INCL as well as rotated component traces, where ORIG_AZM and ORIG_INCL are estimates of the sensor azimuth and inclination during acquisition, and COM_AZIM and COM_INCL are set to the source-borehole azimuth from the surface geometry and ninety degrees for a vertical borehole respectively.

Figure 3 shows that the difference between estimates of sensor azimuth for the principal component and maximum power methods is +/-5 degrees when the default five degree window is used. Estimated angles are ambiguous since the angle that maximizes power on the radial component trace can result in a normal or reversed polarity trace. In fact, the angles stored in ORIG_AZIM turn out to be the estimated angle plus or minus some multiple of 180 degrees. This effect has been removed from the data before plotting Figures 3-5 and creating Table 2. All radial and transverse component source gathers shown in this report have had trace polarity reversals manually picked and applied after component rotation.

Figure 4 shows differences between azimuths estimated by the peak vector amplitude and principal component methods. The differences (uncertainties) are largest for sources closer to the well, and for noisy traces. Figure 5 shows differences for dynamite and Vibroseis sources for all three rotation methods. The Vibroseis data for source point 12 has a series of noisy traces at deeper receiver levels, which are significantly less noisy on the equivalent dynamite data. These show up nicely as greater differences in azimuth when compared to those estimated from the dynamite data (red ellipses, Figure 5). Table 2 shows statistics for Figures 3-5.

a)

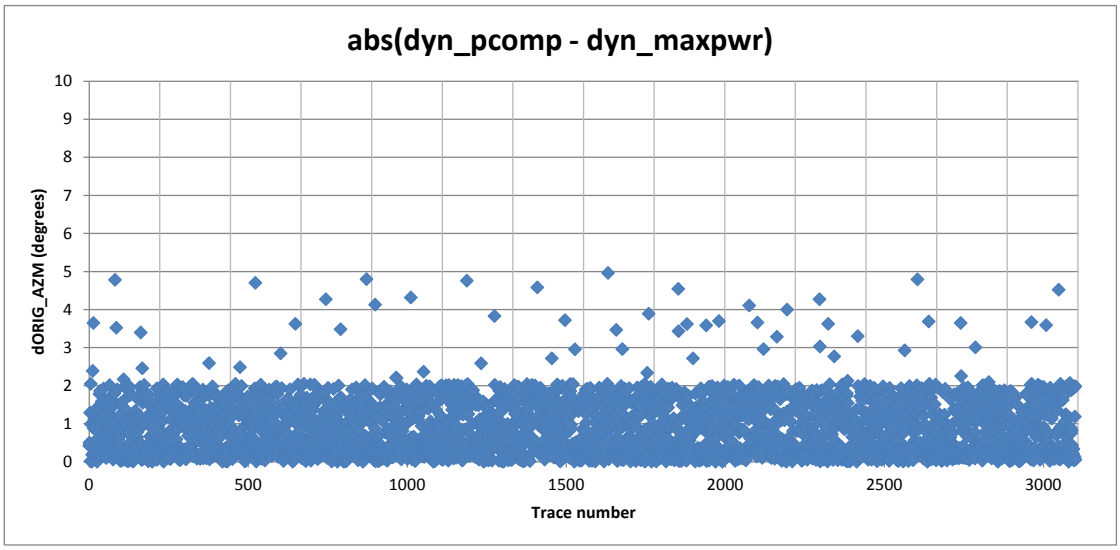

b)

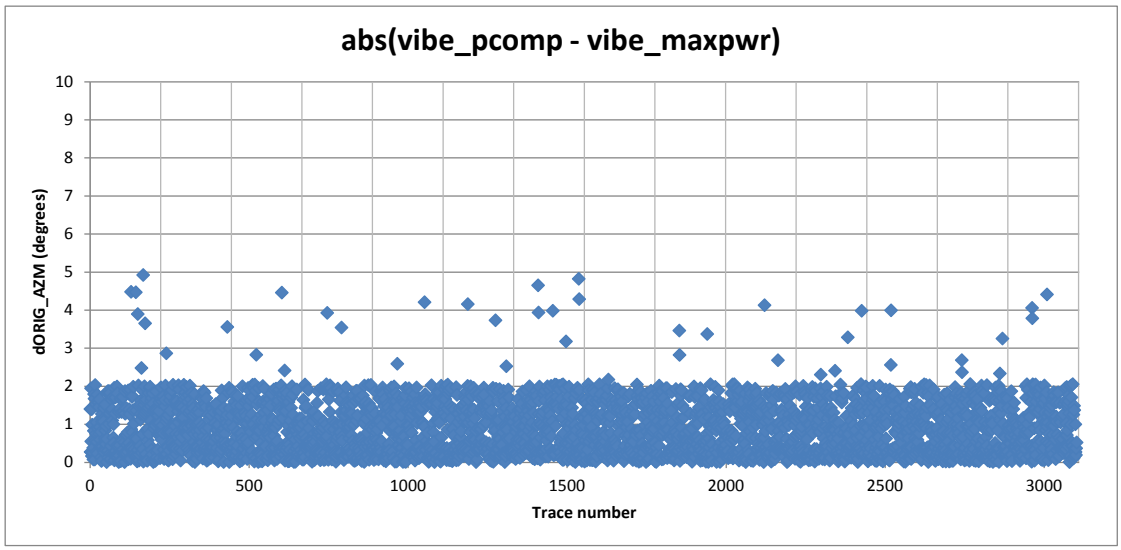

FIG. 3. Difference between receiver orientation azimuths estimated by principal component and maximum power methods for dynamite (a) and Vibroseis (b) sources. Source 1 is on the left, source 14 is on the right. Source gathers are separated by vertical grid lines. The shallowest receiver is on the left side of each source gather.

a)

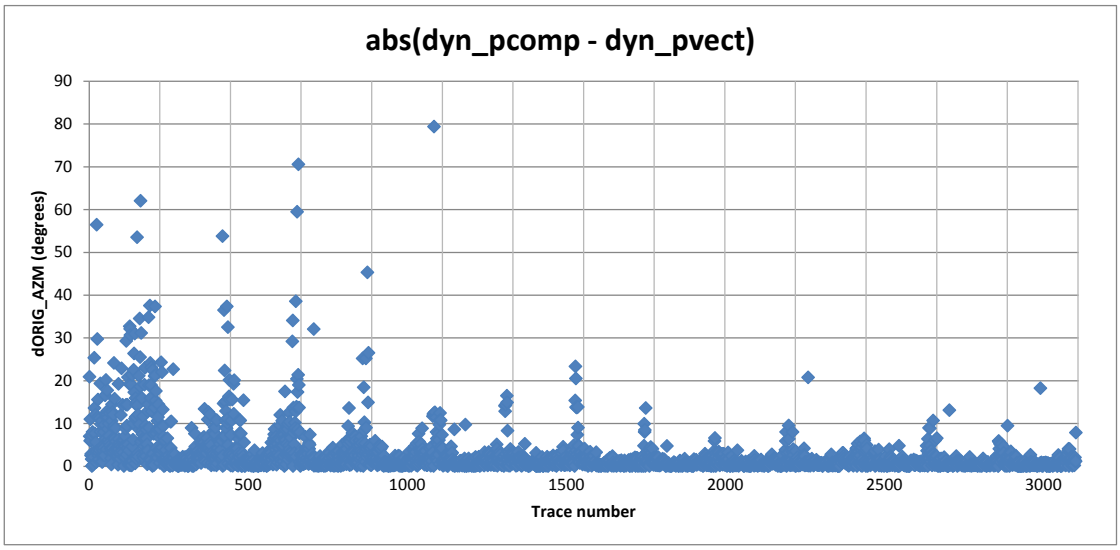

b)

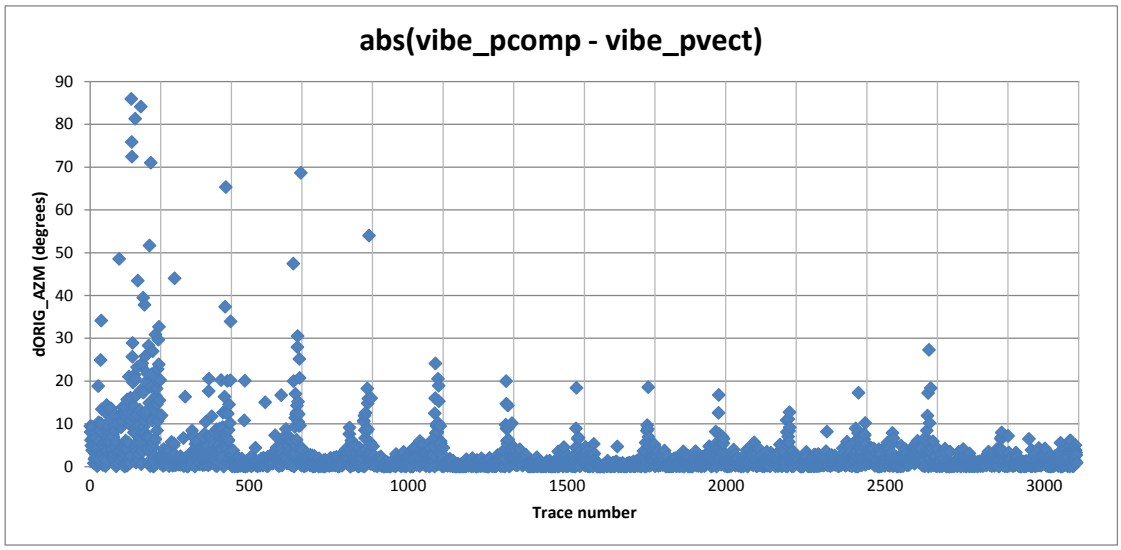

FIG. 4. Difference between receiver orientation azimuths estimated by principal component and peak vector amplitude methods for dynamite (a) and Vibroseis (b) sources. Source 1 is on the left, source 14 is on the right. Source gathers are separated by vertical grid lines. The shallowest receiver is on the left side of each source gather.

a)

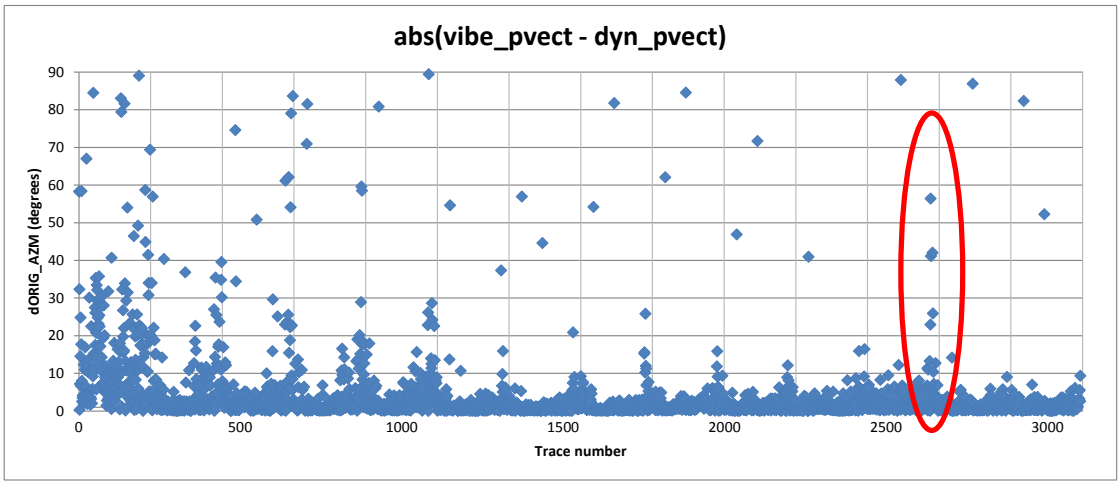

b)

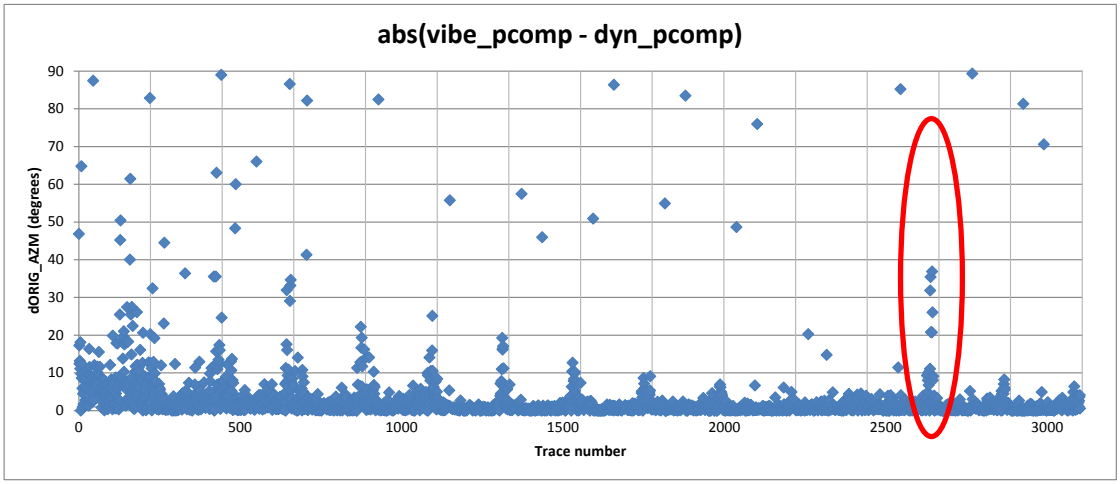

c)

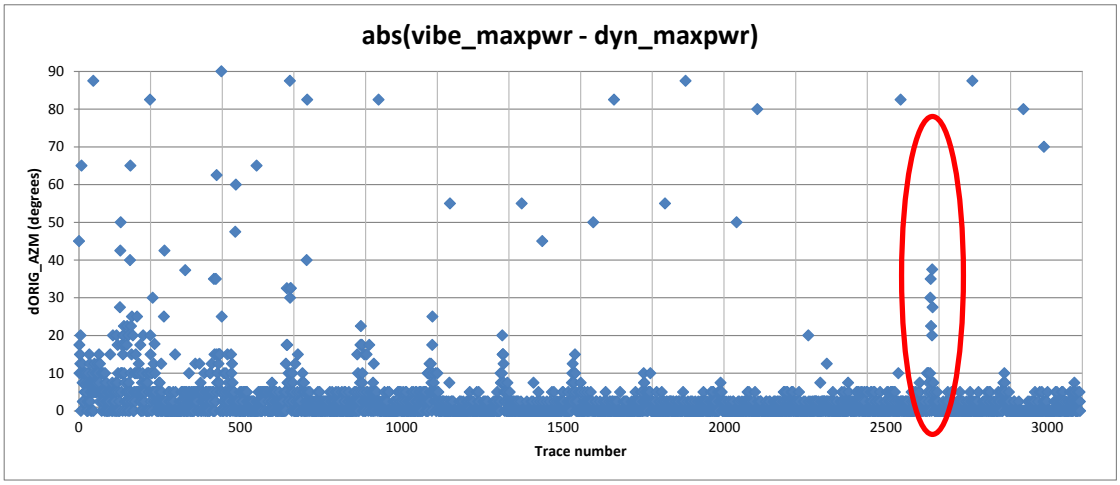

FIG. 5. Difference between receiver orientation azimuths estimated by peak vector amplitude (a), principal component (b) and maximum power (c) methods for dynamite and Vibroseis sources. Source 1 is on the left, source 14 is on the right. Source gathers are separated by vertical grid lines. The shallowest receiver is on the left side of each source gather. Noisy traces observed on Vibroseis data that are quiet on the dynamite data for source 12 result in larger differences in estimated azimuth (red ellipses) than seen on neighbouring traces.

Table 2. Statistics. Minimum, maximum, mean, median and standard deviation of differences in estimated receiver orientation azimuth before component rotation for: Dynamite source, principal component and maximum power (column A, cf. Figure 4a), principal component and peak vector amplitude (column B, cf. Figure 5a); Vibroseis source, principal component and maximum power (column C, cf. Figure 4b), principal component and peak vector amplitude (column D, cf. Figure 5b); Peak vector amplitude method, Vibroseis and dynamite sources (Column E, cf. Figure 6a); Principal component method, Vibroseis and dynamite sources (Column F, cf. Figure 6b); Maximum power method, Vibroseis and dynamite sources (Column G, cf. Figure 6c). Total number of samples is 3104.

	Dyn pcomp-maxpwr (A)	**Dyn** pcomp-pvect (B)	**Vibe** pcomp-maxpwr (C)	**Vibe** pcomp-pvect (D)	**Pvect** Vibe-Dyn (E)	**Pcomp** Vibe-Dyn (F)	**Maxpwr** Vibe-Dyn (G)
min	0.0	0.0	0.0	0.0	0.0	0.0	0.0
max	5.0	79.3	4.9	85.9	89.4	89.4	90.0
mean	0.9	2.5	0.9	2.6	3.9	2.8	2.7
median	0.8	0.9	0.8	1.0	1.3	1.0	0.0
stddev	0.7	5.2	0.7	5.8	9.2	7.5	7.6

The data

Data from source point one is shown in Figure 6 for the dynamite and EnviroVibe sources. This figure presents a visual comparison of the vertical, horizontal, radial and transverse components. In general, the EnviroVibe data are ringy, and noisier than the dynamite data. Visually, there appears to be no difference between the peak vector amplitude and principal component rotation methods at this scale. The direct arrival energy has clearly been concentrated on the vertical and radial components. However, significant S-wave energy is present on both the radial and transverse components. Down-going P (red lines) is clearly observed to result in reflected (up-going; blue lines) and transmitted (down-going; green lines) S wavefields. Down-going source-generated S-waves are visible on all components for both source types, but is noticeably stronger on the EnviroVibe data.

Averaged amplitude spectra for all traces show the influence of source type (Figure 7). The dynamite data contains more high and low frequencies than the EnviroVibe data, which are inherently band-limited by the sweep. Interestingly, there is a 60 Hz spike in the EnviroVibe data that is much less prominent in the dynamite spectra. Figures 8 and 9 show vertical and radial component data for all source points in the survey after component rotation has been applied. Red and green lines show the approximate onset of source-generated P and S direct arrivals, with one pick per source gather. A plane-wave (head-wave) is the first arrival on the far offset gathers (sources 13 and 14). While stronger source generated S-wave energy is observed on near-offset radial component gathers for the EnviroVibe source, this is less obvious for farther offset shots. However, S-wave energy can also be clearly observed on the vertical component data at farther offsets.

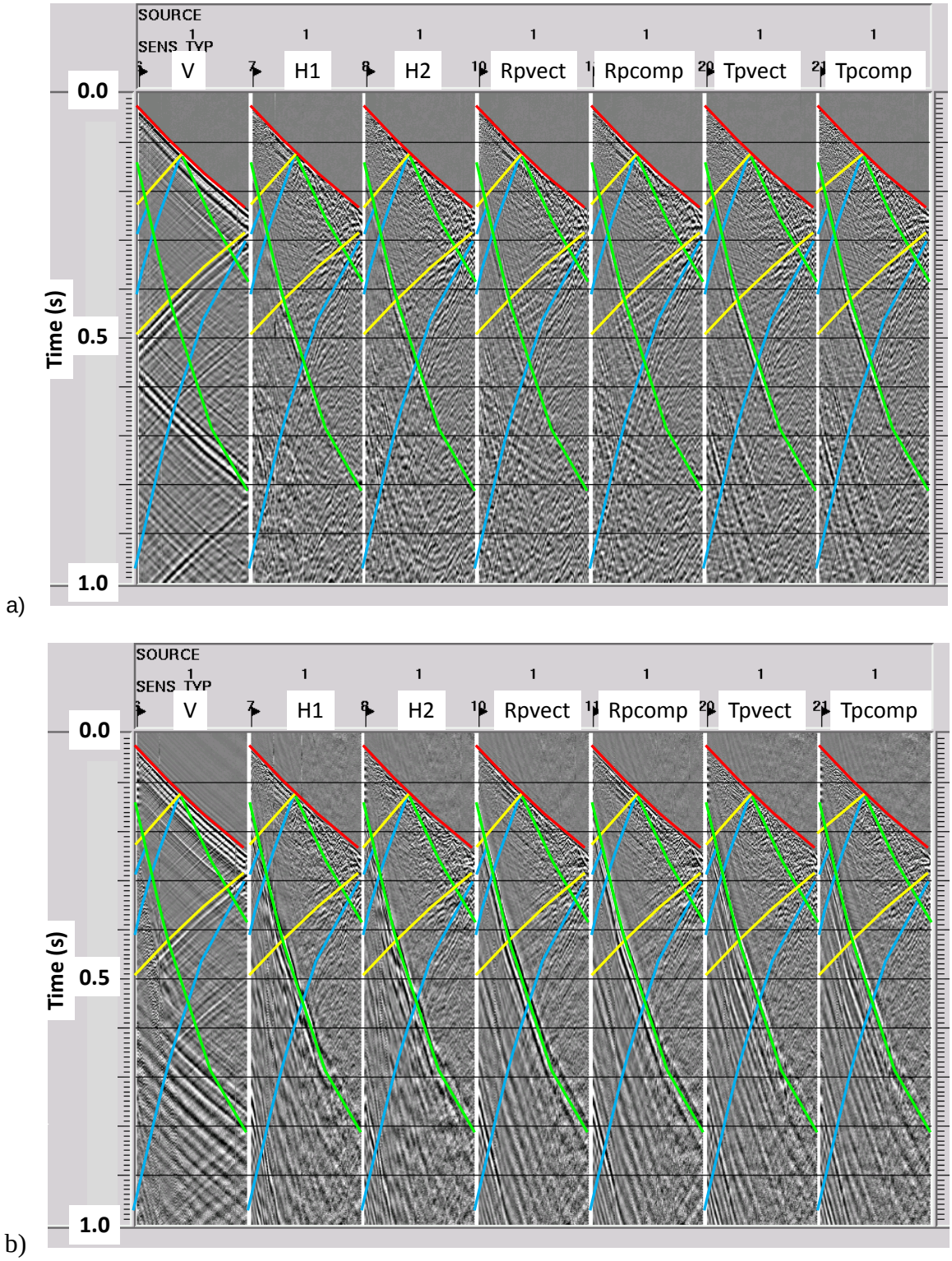

FIG. 6. Dynamite (a) and Vibroseis (b) data for source point 1. From left to right: vertical component, horizontal 1, horizontal 2, radial from peak vector amplitude method, radial from principal component method, transverse from peak vector amplitude method, and transverse from principal component method, with 500 ms AGC for display. Red lines are P-downgoing, yellow is P-upgoing, green is S-downgoing, and blue is S-upgoing.

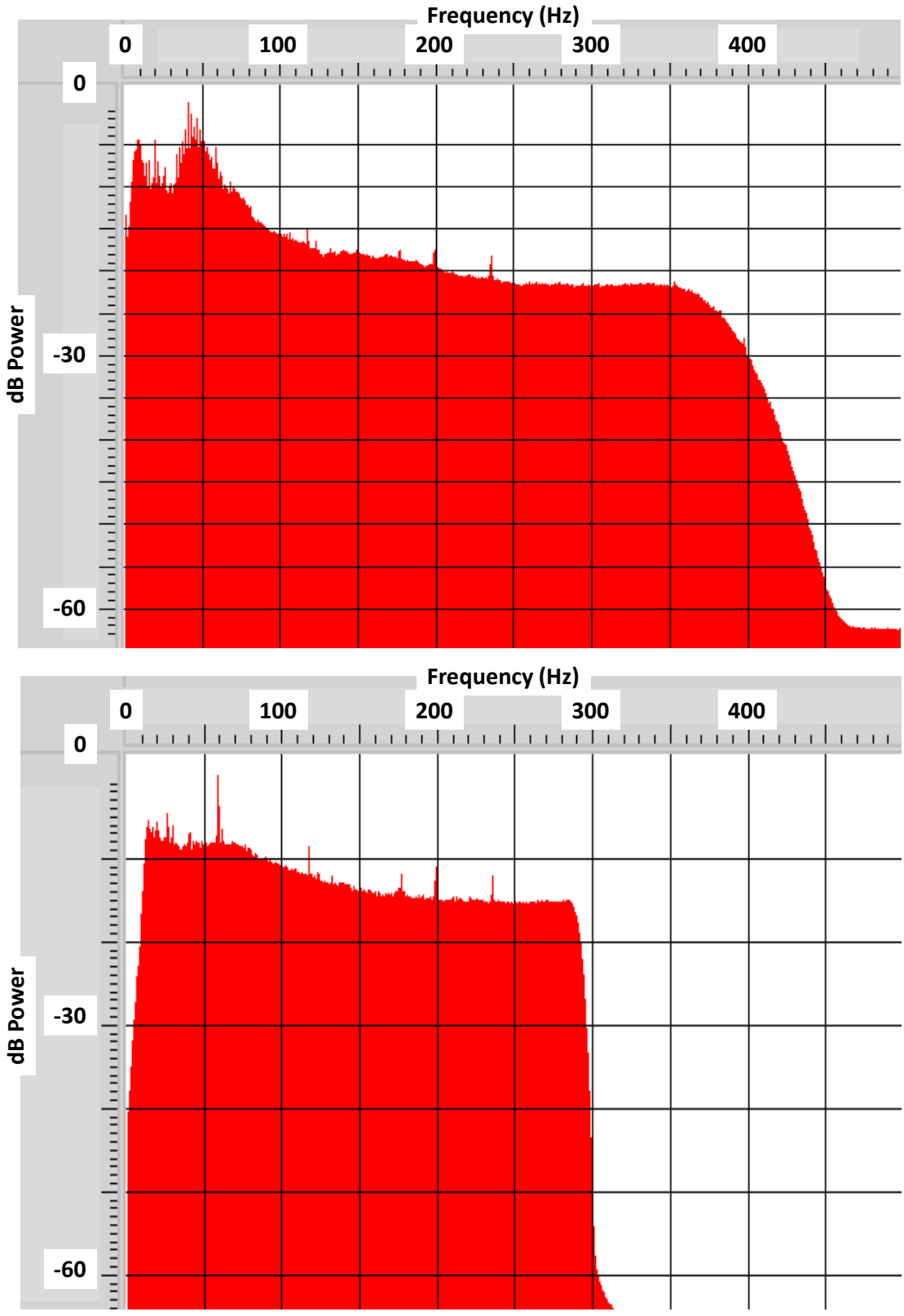

FIG. 7. Averaged amplitude spectra for all traces of the (a) dynamite and (b) Envirovibe data.

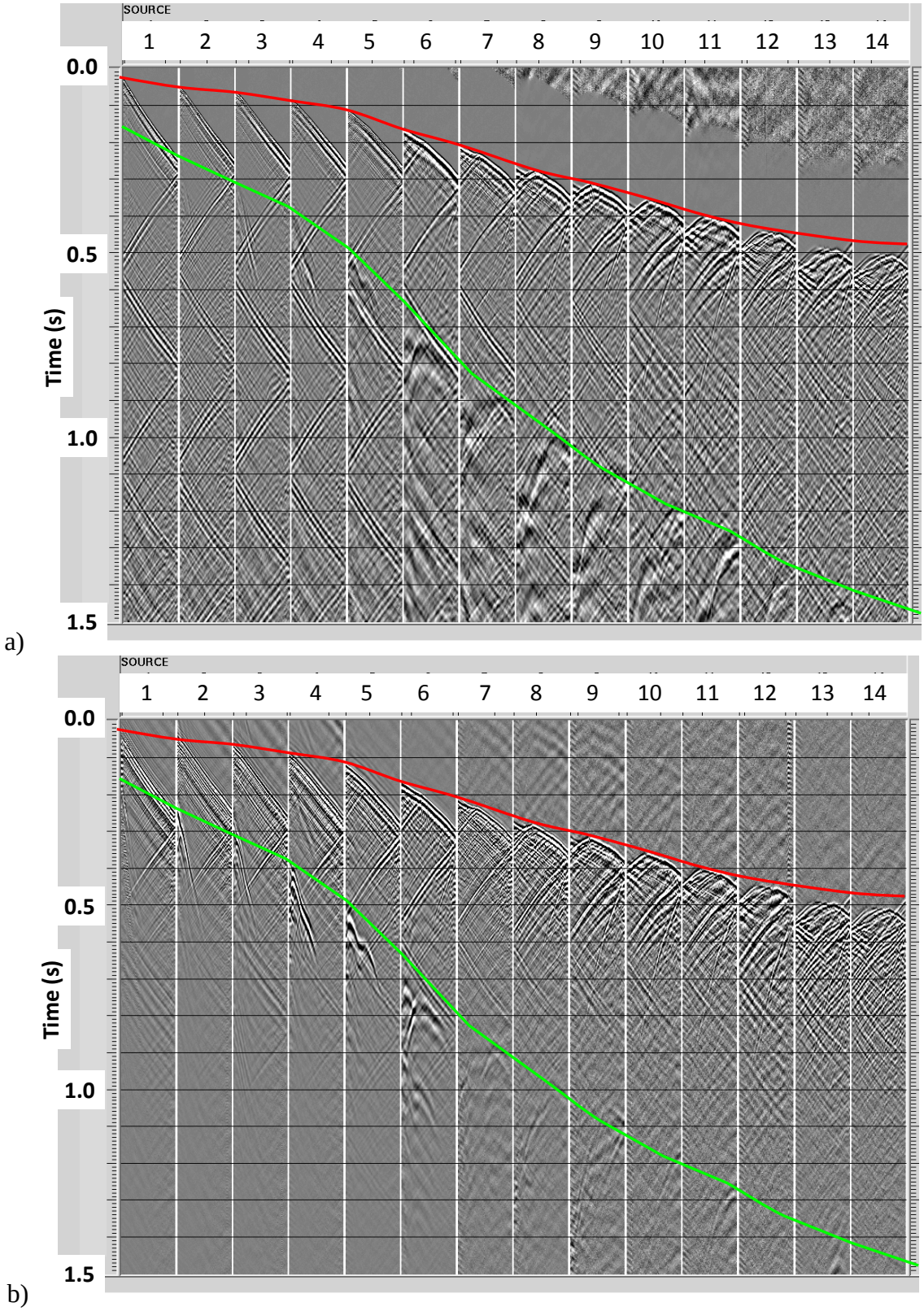

FIG. 8. Dynamite (a) and Vibroseis (b), vertical component gathers for all shots with 500 ms AGC for display. Red line is approximate time of first P-downgoing first arrival, one pick per shot gather. Green line is S-downgoing,

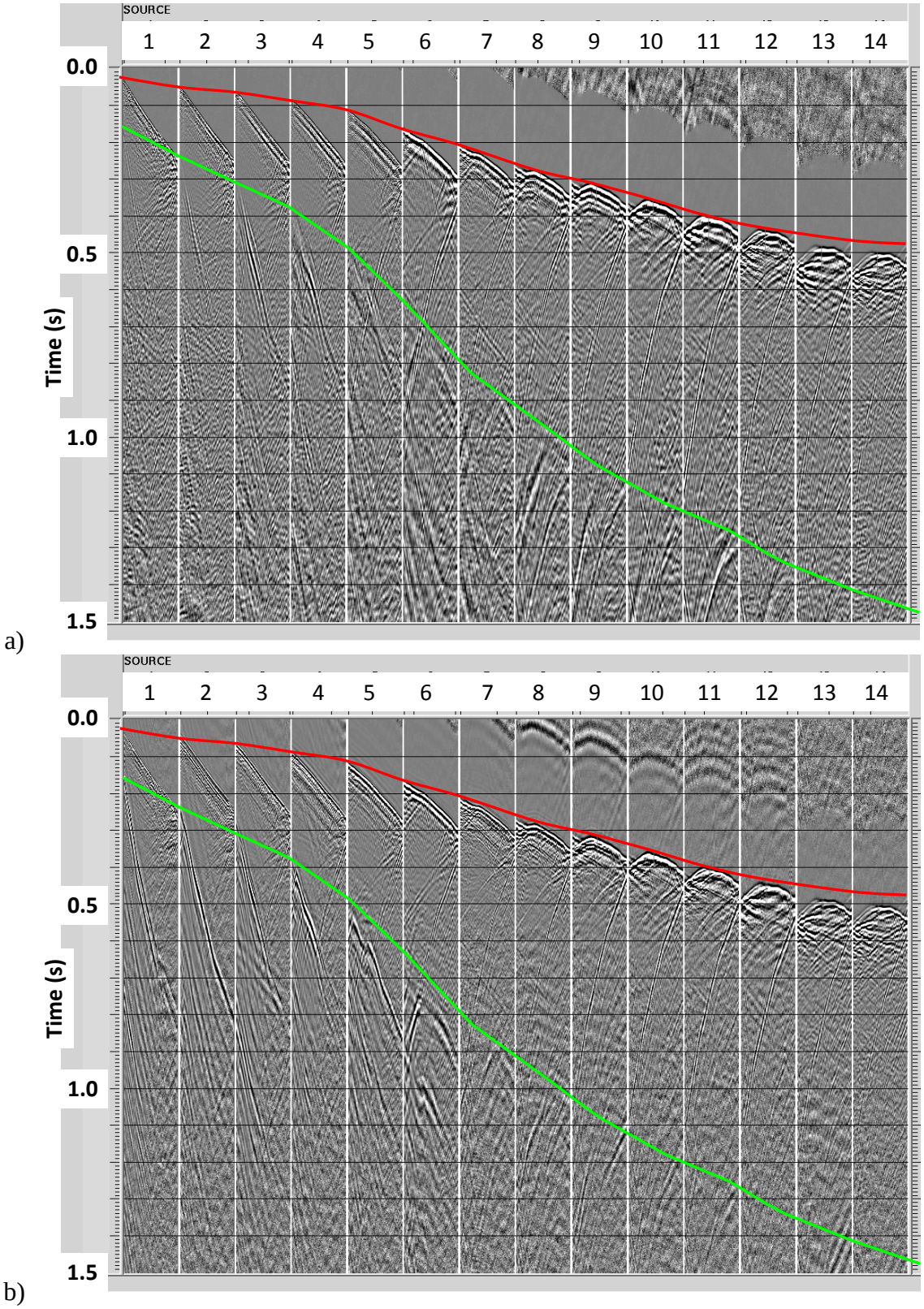

FIG. 9. Dynamite (a) and Vibroseis (b), radial component gathers for all shots, with 500 ms AGC for display. Red line is P-downgoing first arrival, one pick per shot gather. Green line is S-downgoing.

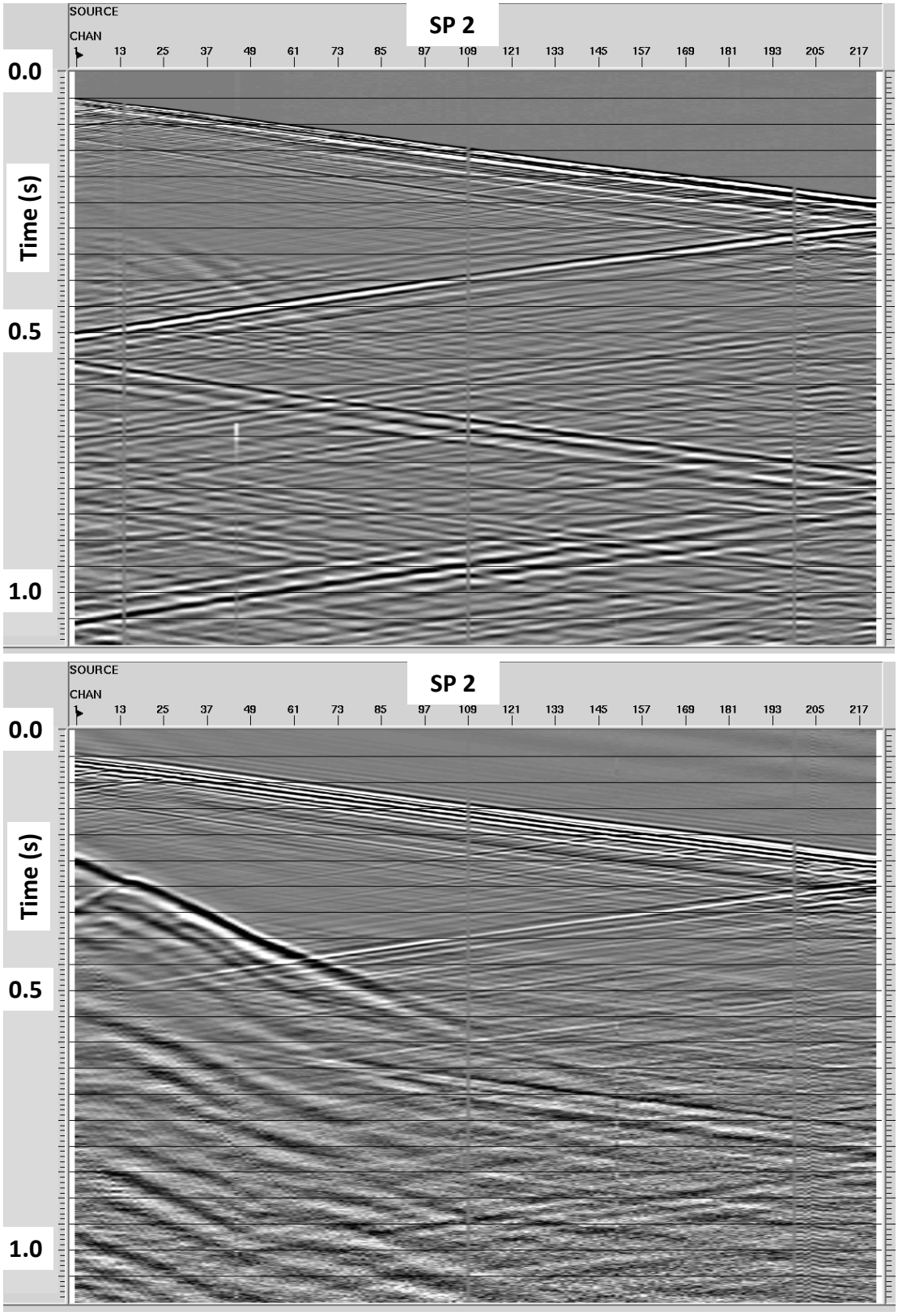

FIG. 10. Visual comparison of vertical component records for dynamite (a) and EnviroVibe (b) sources at source point 2.

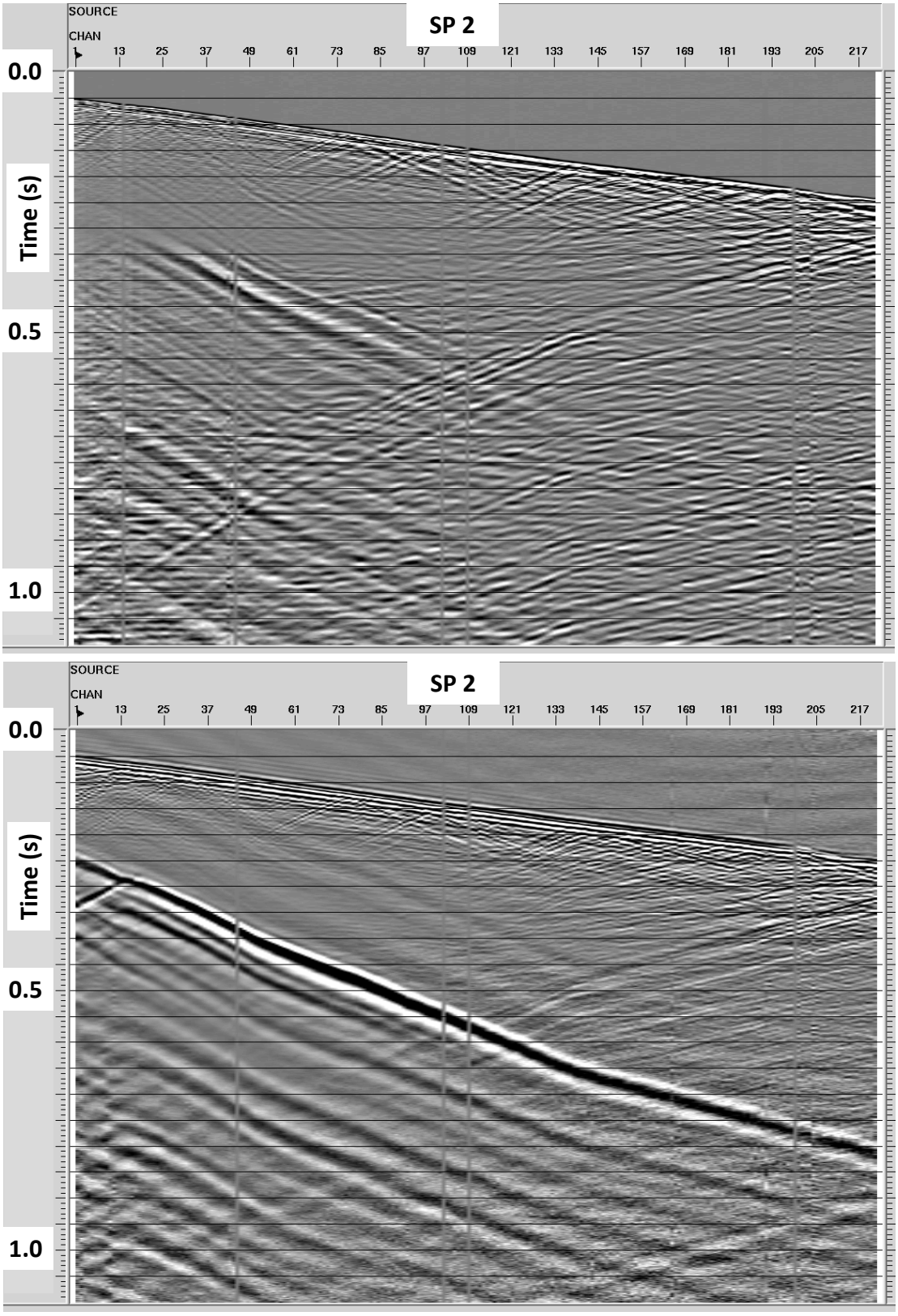

FIG. 11. Visual comparison of radial component records for dynamite (a) and EnviroVibe (b) sources at source point 2.

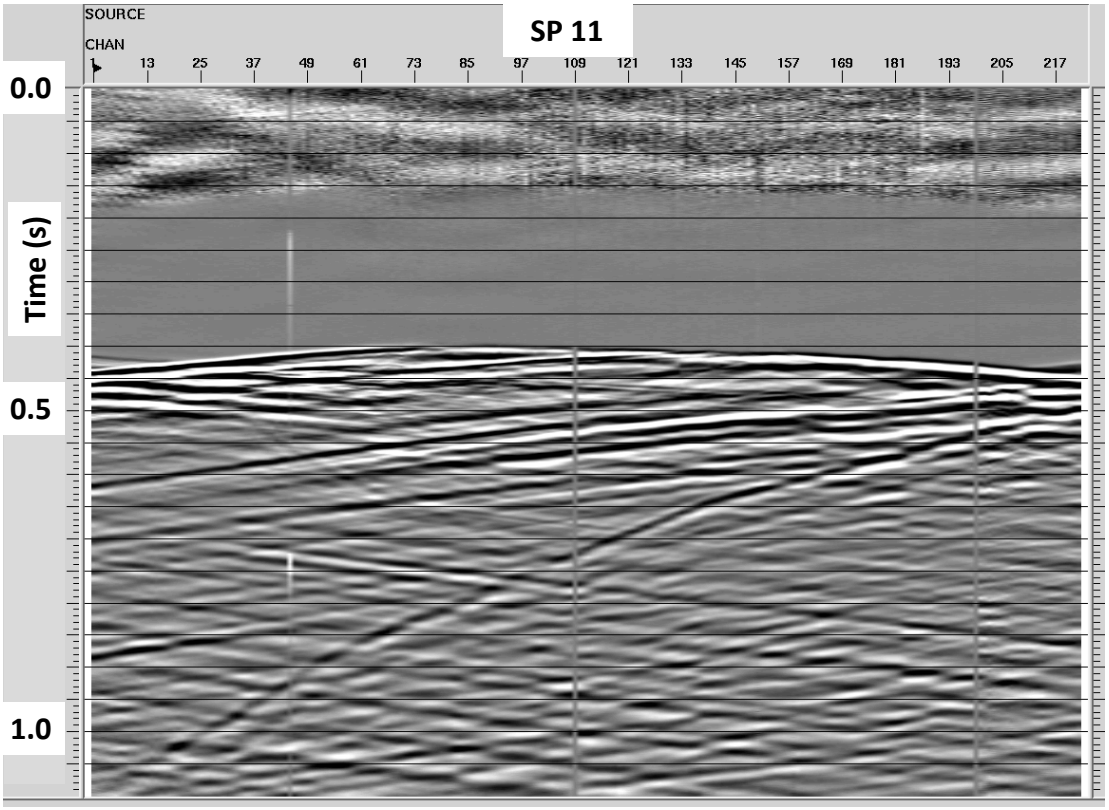

a)

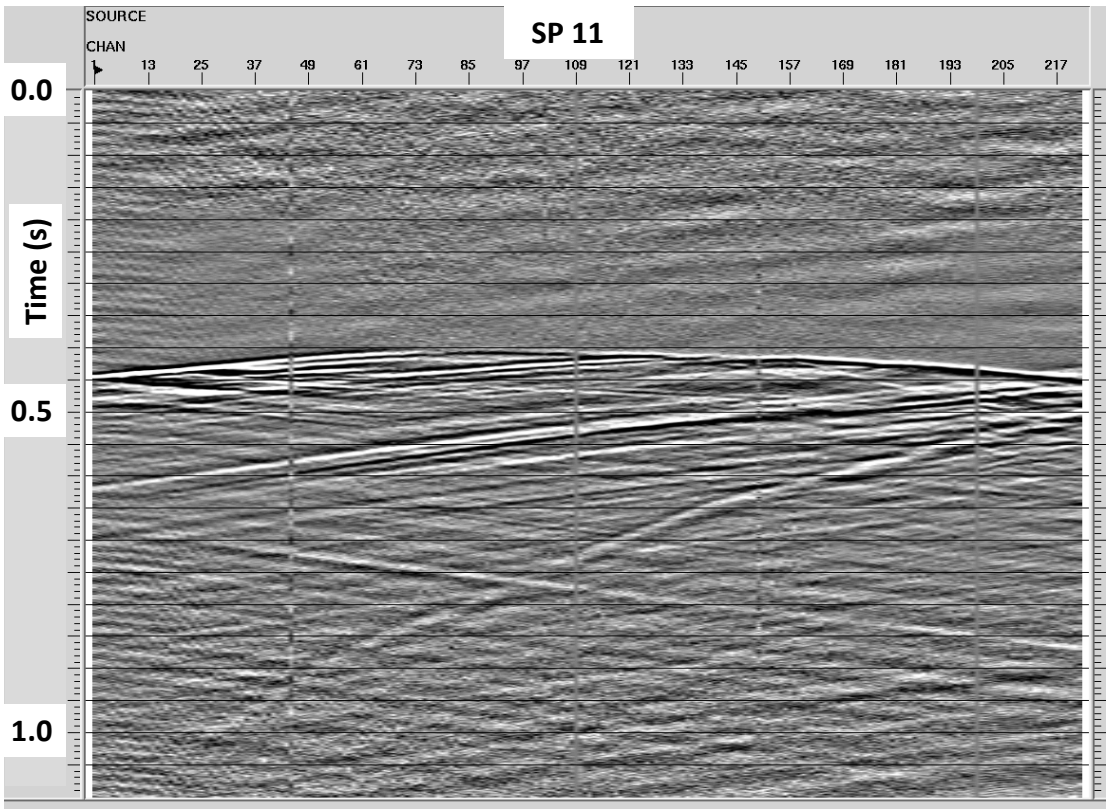

b)

FIG. 12. Visual comparison of vertical component records for dynamite (a) and EnviroVibe (b) sources at source point 11.

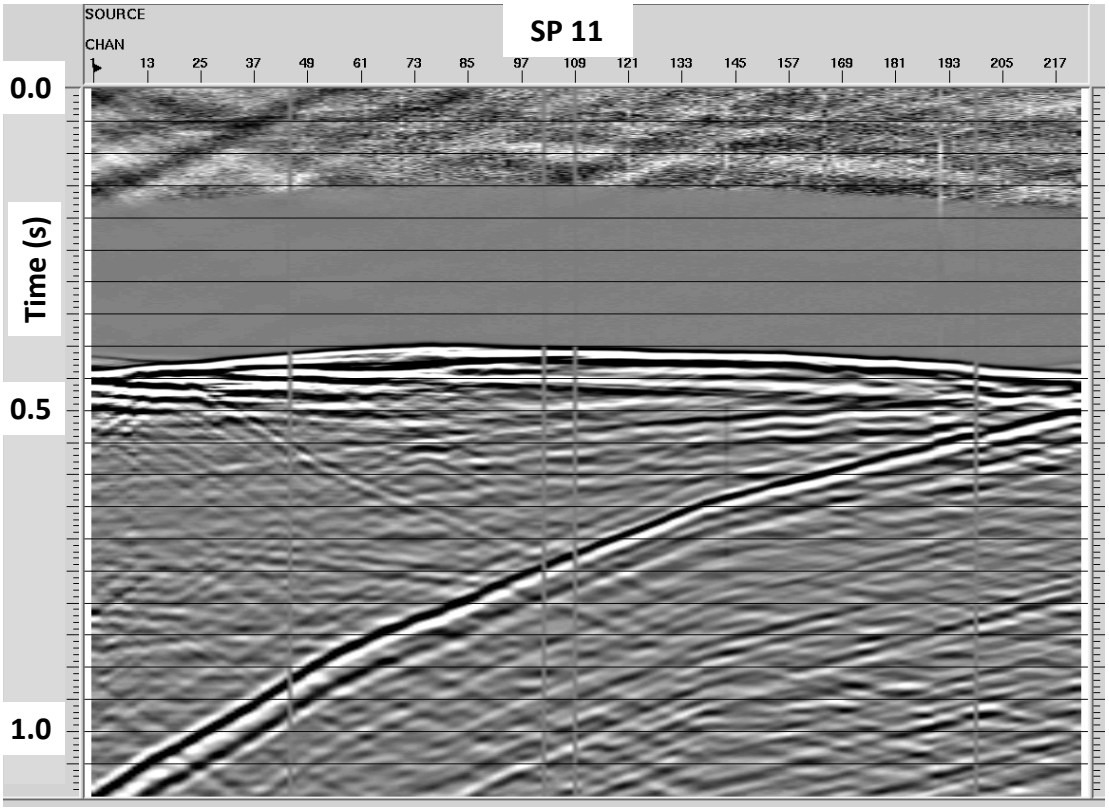

a)

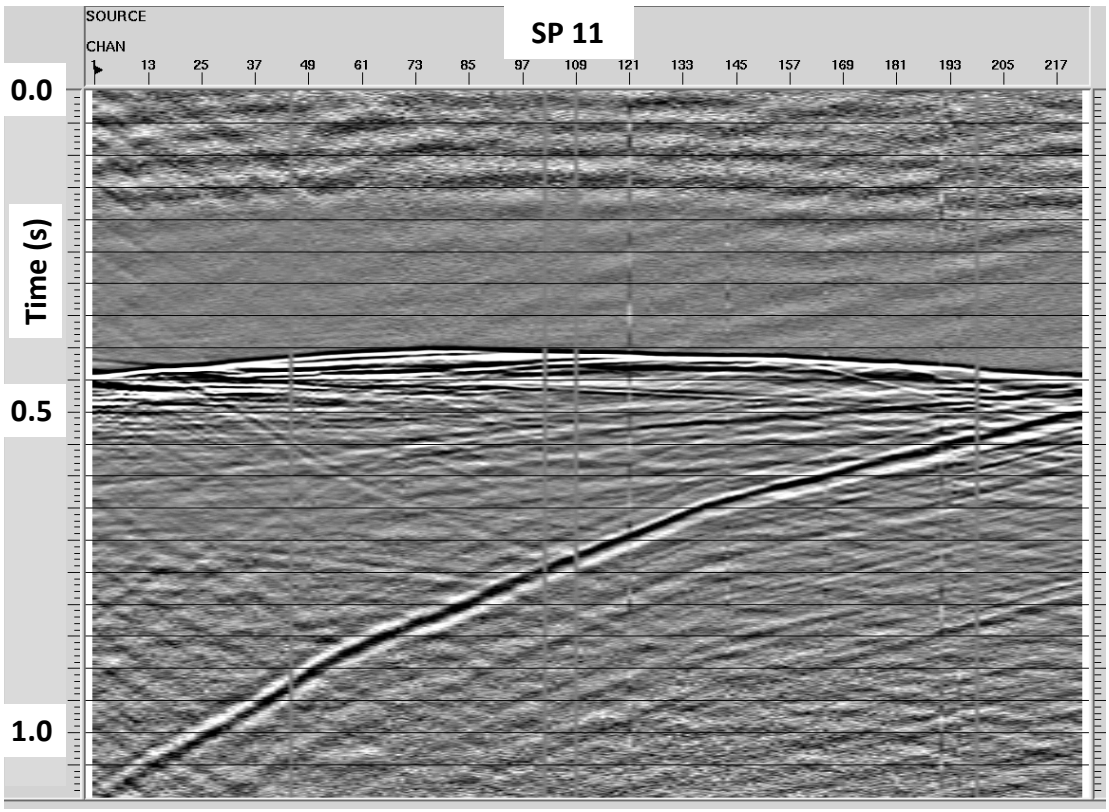

b)

FIG. 13. Visual comparison of radial component records for dynamite (a) and EnviroVibe (b) sources at source point 11.

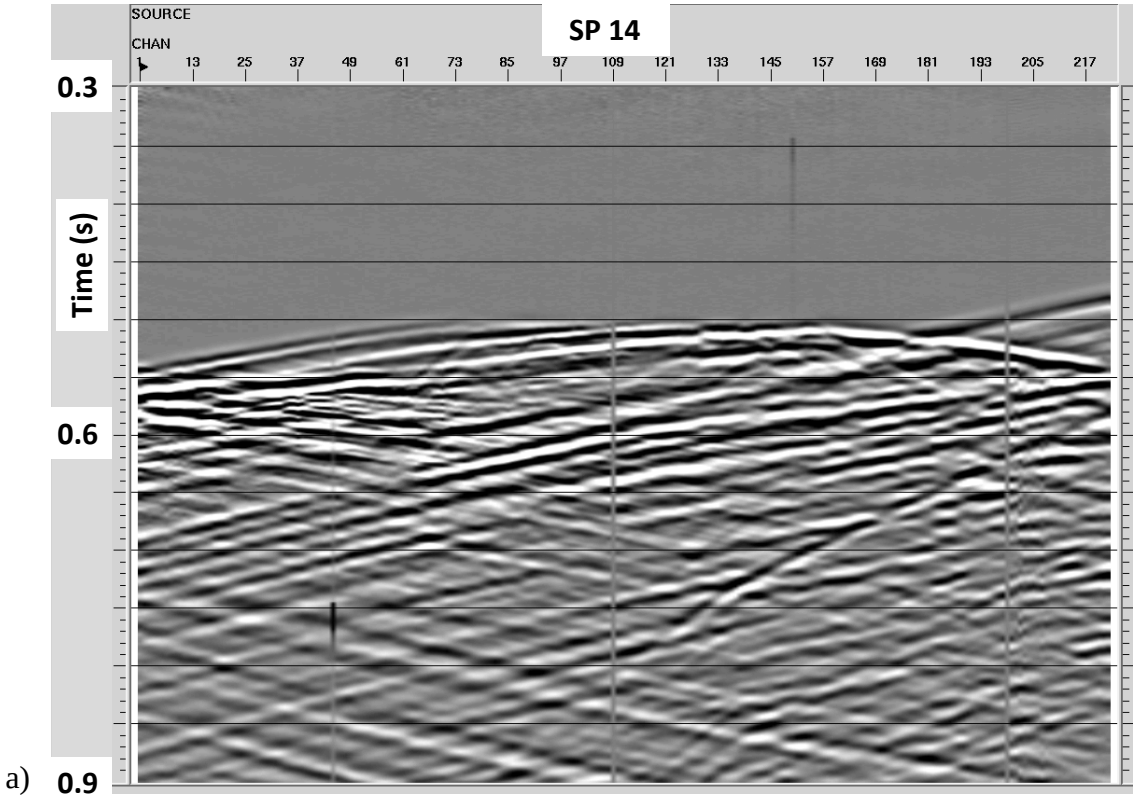

a)

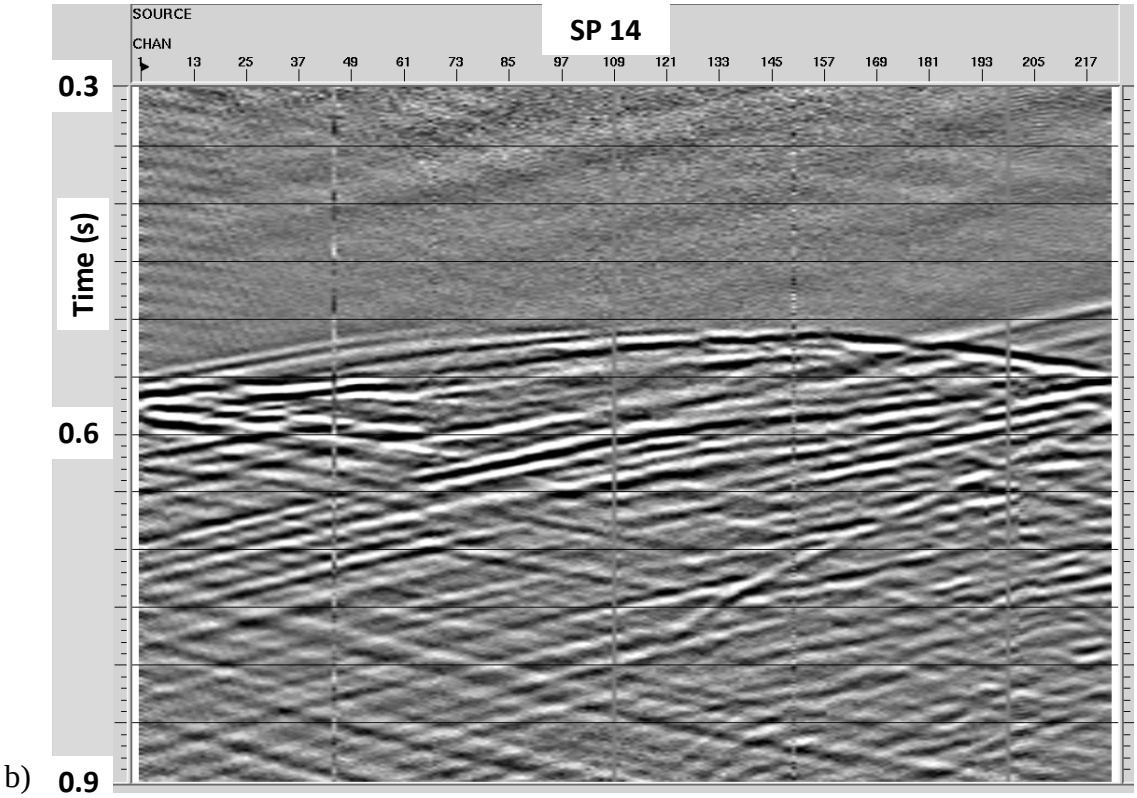

b)

FIG. 14. Visual comparison of vertical component records for dynamite (a) and EnviroVibe (b) sources at source point 14.

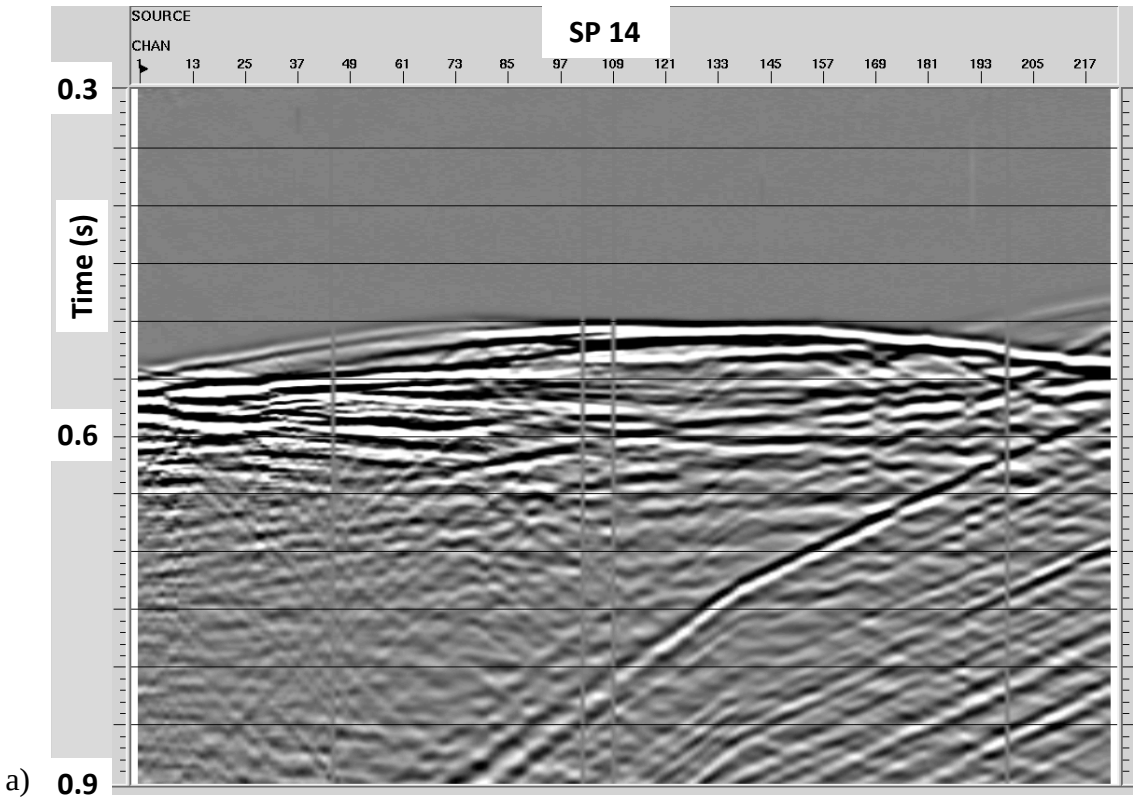

a)

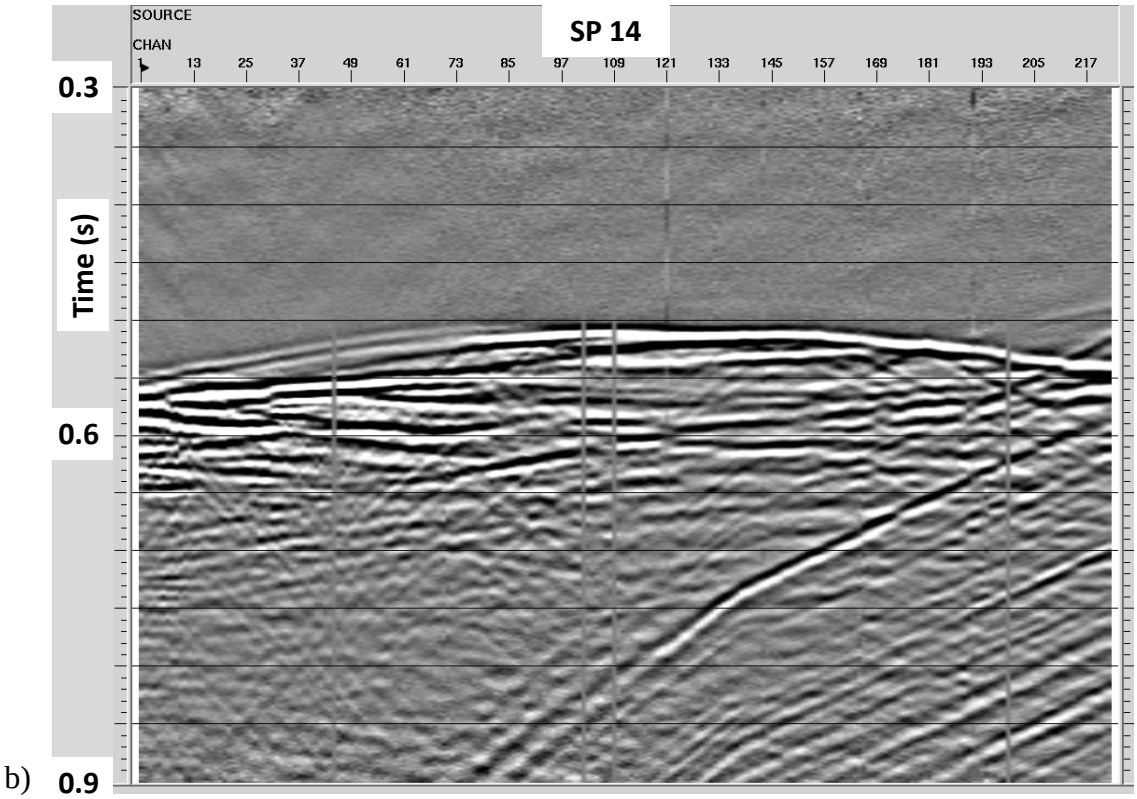

b)

FIG. 15. Visual comparison of radial component records for dynamite (a) and EnviroVibe (b) sources at source point 14.

Figures 10-15 show more detailed visual comparisons of the vertical (Figures 10, 12 and 14) and radial components (Figures 11, 13 and 15) for source points 2, 11, and 14 for dynamite and EnviroVibe Sources. These records illustrate the rich elastic wavefield present in these data.

Wavefield separation and corridor stack

The initial processing flow for wave-field separation and corridor stack for the vertical component followed the standard practice of flattening on first-break picks (apply first-break pick as a static shift to the traces), median filtering to enhance down-going P, and subtraction of this result from the flattened result to remove down-going P. Figure 16 shows the result of applying this processing to the vertical and radial components of dynamite source point one. Reflected and transmitted converted-wave S events are clearly visible on the radial component, as well as source generated down-going S direct arrivals, and up-going S reflections (Figure 16b).

The vertical component gather was then flattened on up-going P reflections by applying the first-break picks as a static shift again (greyscale seismic display, Figure 17a), and after application of top and bottom mutes was stacked to produce a P-P corridor stack (black traces, Figure 17a). As the direct-S arrival could not be picked for the entire gather, a prominent up-going S reflection that was visible on all traces was picked on the radial component gather (Figure 16b), and used to flatten the up-going S wavefield. Traces were then aligned in a window centred on the flattened pick, and an *f-k* filter was applied to reject all dipping events (greyscale seismic; Figure 17b). Top and bottom mutes were picked and the gather was stacked to produce a P-S corridor stack (black traces; Figure 17b).

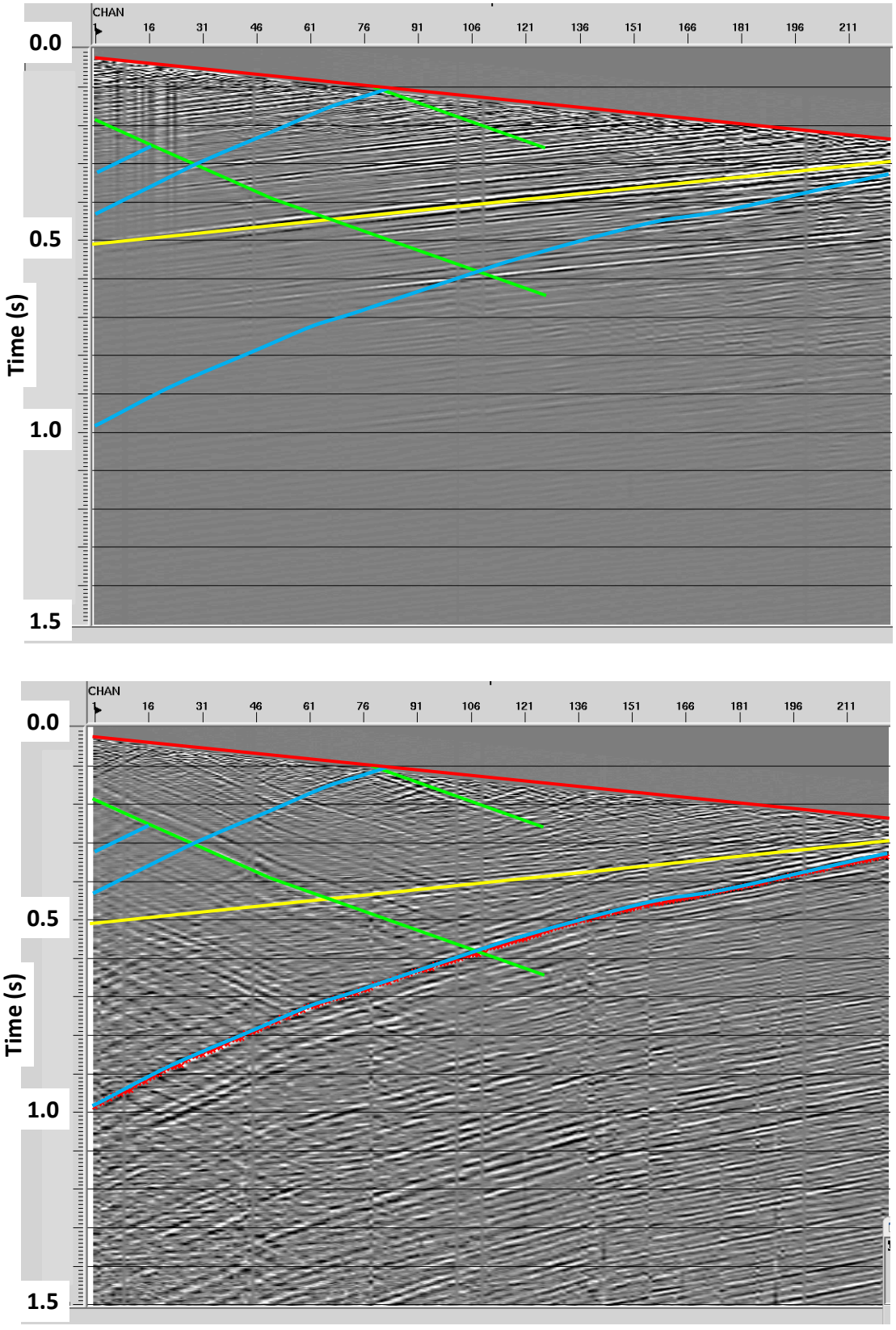

FIG. 16. Vertical (a) and radial (b) components for dynamite source point 1, after removal of down-going P (red line). Yellow denotes up-going P, green down-going S, and cyan up-going S.

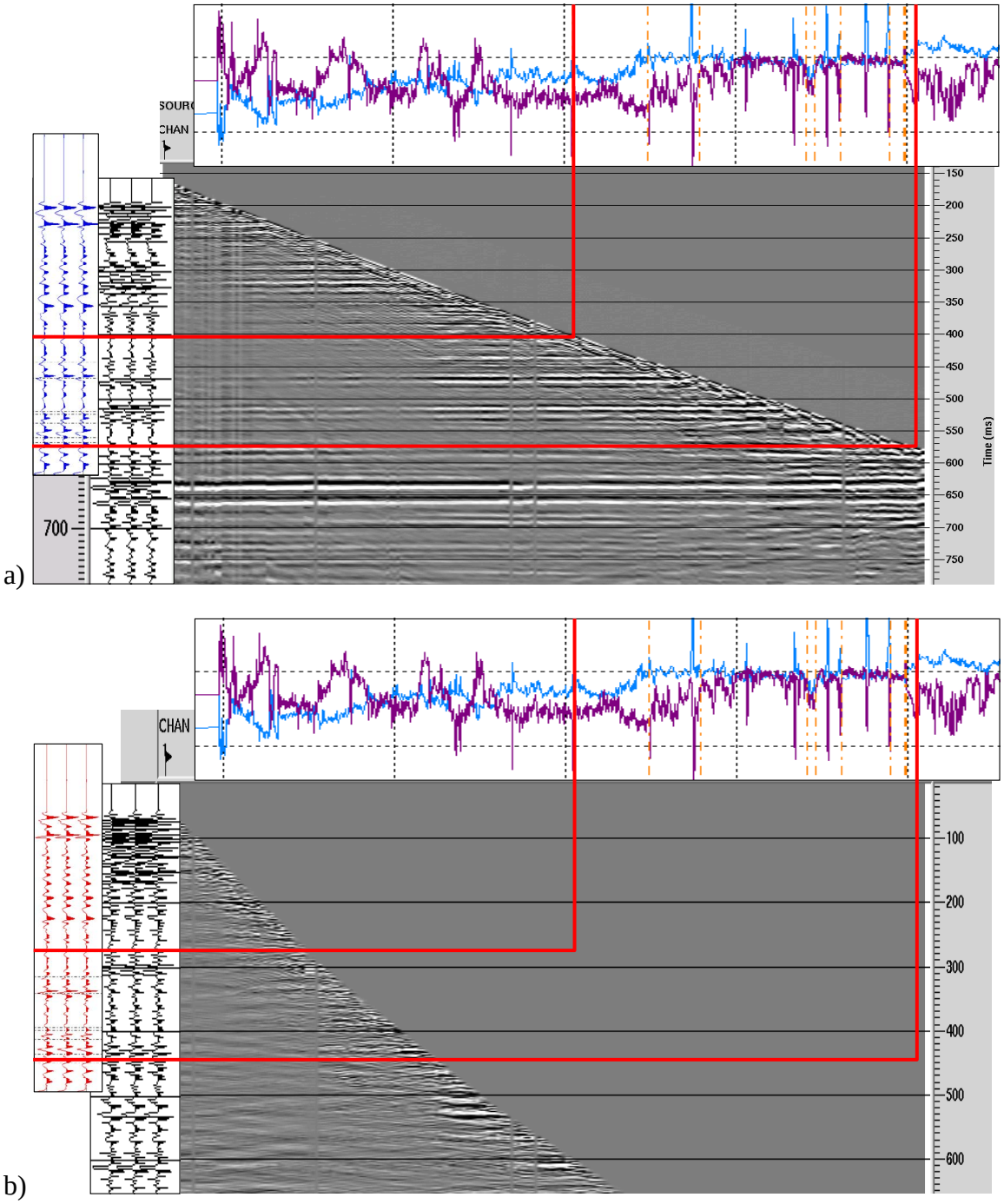

FIG. 17. Dynamite, vertical (a) and radial (b) components. Blue and red traces are P-P and P-S synthetic seismograms (repeated 3x), black traces are corridor stacks (repeated 3x), grayscale seismic data is up-going P (a) and up-going S (b), purple and cyan curves are the density and P-sonic logs from a nearby well. Vertical scale is one-way P-travel time. Horizontal scale is depth.

Initial interpretation

P-wave sonic (cyan; Figure 17) and density (purple; Figure 17) logs are available from a nearby well, about 200 m away. CREWES Syngram was used to generate P-P (blue traces; Figure 12) and P-S (Red traces) synthetic seismograms from these logs, using a simulated impulsive source 50 Hz dominant frequency minimum phase wavelet. The up-going P and up-going converted-wave S gathers can be used to map depth to one-way P-travel-time (red lines, Figure 17). Note that while the vertical time scale is the same for Figures 17a and 17b, the events no longer line up at the same time in the image. This is due to bulk-shifting of the up-going converted-wave S during flattening, that has yet to be corrected. The synthetic seismograms have been stretched to one-way P-travel-time, based on the red L-shaped lines shown in Figure 17, and encouragingly, don't appear to be entirely dissimilar to the corridor stacks.

FUTURE WORK

Seismic attenuation (Q) can be estimated from VSP data. The parameter Q is a quantity which is rarely measured but is of great applications to analysis of seismic data. If Q is a known quantity then inverse Q filtering can be used to increase the resolution of a seismic data set. Also, knowing the value of Q would allow for the correction of any amplitude distortions that arise from attenuation, which would allow for more accurate AVO analysis. Finally, Q is sensitive to lithology, porosity, and fluid saturation, so it can be a useful tool for seismic interpretation.

Zero offset VSP data lends itself well to several methods of estimating Q due to its geometry. There are several methods which can be used to estimate Q from VSP data, many of which were compared by Tonn (1991). Tonn came to the conclusion that when true amplitude recordings are available, the analytical signal method (Englehard, 1996) is superior. If true amplitude recordings are not available then the spectral-ratio method (Bath, 1974) is best in the noise free case. Both of these methods for estimating Q will be applied to this heavy oil VSP data and then compared against each other and against the match filter method for estimating Q which was developed by Cheng and Margrave (2011). Q_p will be determined using the downgoing P-wave and Q_s will be determined using the upgoing S-wave.

Analytic signal method

A seismic trace can be described by an instantaneous amplitude and phase (Taner et al, 1979):

$$x(t) = a(t)cos\varphi(t). \tag{1}$$

A quadrature trace can then be defined as:

$$y(t) = ia(t)sin\varphi(t), \tag{2}$$

where $x(t)$ and $y(t)$ are a Hilbert transform pair. The complex trace can then be expressed as:

$$z(t) = a(t)e^{i\varphi(t)} = x(t) + iy(t). \quad (3)$$

The instantaneous angular frequency $\omega(t)$, is the time derivative of the instantaneous phase (Englehard, 1996):

$$\omega(t) = \frac{d\varphi(t)}{dt}. \quad (4)$$

Since the instantaneous amplitude and phase can be expressed in terms of *x(t)* and *y(t)* as follows:

$$a(t) = x(t)^2 + y(t)^2 = z(t)z^*(t), \quad (5)$$

$$tan\varphi(t) = \frac{y(t)}{x(t)} = \frac{(z - z^*)}{i(z + z^*)}. \quad (6)$$

where z^* is the complex conjugate of z. From equation 4 and 6 it follows that the instantaneous frequency can be written as:

$$\omega(t) = \frac{d\varphi(t)}{dt} = \frac{z^*z' - zz^{*\prime}}{2izz^*}. \quad (7)$$

Finally, the seismic parameter Q can be found through (Tonn, 1991):

$$\ln\left[\frac{a(t_2)}{a(t_1)}\right] = \ln\left[\frac{G_2}{G_1}\right] - \frac{\Delta t}{4Q}\big(\omega(t_1) + \omega(t_2)\big). \quad (8)$$

where t_1 and t_2 are two different different times, $a(t_2)$ and $a(t_1)$ are instantaneous amplitudes, $\omega(t_1)$ and $\omega(t_2)$ are instantaneous angular frequencies, Δt is the difference between t_2 and t_1, and $G_1$and G_2 are geometric spreading factors. There are three ways in which equation 8 can be used to compute Q (Tonn, 1991). Maxima method, where only the maxima of the instantaneous amplitudes is analyzed, seems to be the best choice, as it does not require correct time synchronization. In this case Δt will be the time from one maxima to the next.

Qp and Qs can be found graphically by assuming a range of Q factors and calculating the corresponding range of log-spreading-factors using equation 8. When these different curves are plotted for a given depth the correct Q and the correct log-spreading-factor will be at the intersection point of the curves (Haase and Stewart, 2004).

Spectral ratio method

If a constant Q model for attenuation is assumed (Aki and Richards, 1980) then Q can be expressed through:

$$A_1(\omega) = KA_0(\omega)e^{-\frac{\omega t}{2Q}}. \tag{9}$$

where A_0 and A_1 are amplitude spectrums, ω is angular frequency, t is time, and K is a constant which represents any energy loss term which is not frequency dependant, including geometrical spreading, reflection, and transmission energy losses. Equation 9 states that some seismic wavelet travelling through the subsurface with amplitude spectrum A_0 will have a different amplitude spectrum some time t, later.

Equation 9 can also be rearranged and written as:

$$\ln\left[\frac{A_1(\omega)}{A_0(\omega)}\right] = \ln(K) - \frac{\omega t}{2Q}, \tag{10}$$

so, if the log-ratio of the amplitude spectra are plotted against frequency and then a linear best fit line will have a slope of which can be expressed in terms of Q.

Match filter method

The match filter method for estimating Q which was developed by Cheng and Margrave (2011) is derived in a similar fashion to the spectral ratio method. However, the spectral ratio method was derived for use with VSP data, while the match filter method can be applied to reflected wave data. Therefore a correction term must be applied to equation 10. Consider a wavelet with a spectrum $S(\omega)$ travelling through a layered media with reflectivity R_1. If the attenuation of the layered medium can be expressed through the constant Q model, then the spectrum can be approximated by (Cheng and Margrave, 2011):

$$|A_1(\omega)| \approx G(t_1)|S(\omega)||R_1(\omega)|e^{-\frac{\omega t_1}{2Q}}. \tag{11}$$

where $R_1(\omega)$ is the reflectivity series associated with time t_1, and $G(t_1)$ is a geometrical spreading factor. In a similar fashion for a time t_2 with reflectivity series $R_2(\omega)$ the amplitude spectrum can be expressed as:

$$|A_2(\omega)| \approx G(t_2)|S(\omega)||R_2(\omega)|e^{-\frac{\omega t_2}{2Q}}. \tag{12}$$

Then, if well log data is available and reflectivity can be calculated equations 11 and 12 can be combined and written as:

$$\ln\left[\frac{|A_2(\omega)/R_2(\omega)|}{|A_1(\omega)/R_1(\omega)|}\right] = \ln\left[\frac{G(t_2)}{G(t_1)}\right] - \frac{\omega\Delta t}{2Q}, \tag{13}$$

which is familiar as the spectral ratio method with a correction term built in.

Since the match filter method was developed to be used with data collected from a reflection survey it would be useful to build a model using the data from the VSP survey and well logs to test the match filter method. The results can then be compared against those which were obtained from the spectral-ratio method. Since the two methods are closely related it is expected that the estimates of Q in each case should be similar. The results of both methods can then be compared to the analytical signal method, which is the best method if true amplitude is recorded (Tonn, 1991).

Finally, an empirical equation relating Q_s and Q_p is given by Udias (1999):

$$Q_s = \frac{4Q_p}{3\left(\frac{V_s}{V_p}\right)}, \tag{14}$$

and it can be used to determine if the values of Q_s obtained through each of the three methods are reliable. V_s and V_p are the S-wave and P-wave velocities and can be determined through well log data and the zero-offset VSP data.

DISCUSSION

The three methods available for automated component rotation in the ProMAX module '3-Component Rcvr Orientation' give very similar results for this dataset based on visual inspection, although the differences in estimated original azimuths can be quite different for noisy traces, and for near-offset source points.

Up-going converted wave shear energy is clearly present on the radial component after component rotation, and can be used to create a P-S corridor stack for the near-zero-offset dynamite shot, which should have the least chance of success for this process. Source generated down-going shear waves can be seen on the vertical, radial and transverse components. Up-going S-S reflections can also be seen.

This is a high-quality, very rich dataset, that will afford many opportunities for future research, including attenuation studies based on both up-going and down-going wave-fields. To date, no true amplitude recovery, deconvolution, or filtering has been applied to the data. The walk-away VSP has not yet been processed to an image via VSP-CDP transform.

ACKNOWLEDGEMENTS

The authors would like to thank Husky Energy for giving us the opportunity to participate in this experiment, and for giving us permission to show our results, High Definition Seismic and Geokinetics for their help in the field, and Landmark Graphics for the use of donated ProMAX software.

REFERENCES

Aki, K. and Richards, P. G., 1980, Quantitative Seismology, second edition: University Science Books

Bath, M., 1974, Spectral Analysis in Geophysics: Developments in Solid Earth Geophysics, Vol. 7: Elseveir Science Publishing Co.

Cheng, P. and Margrave, G., 2011, Q estimation by a match-filter method: CREWES Research Report, 23.
Englehard, L., 1996, Determination of seismic-wave attenuation by complex trace analysis: Geophysics Journal International, 125, 608-622.
Haase, A. and Stewart, R., 2003, Q-factor estimation from borehole seismic data: Ross Lake, Saskatchewan: CREWES Research Report, 15.
Haase, A. and Stewart, R., 2004, Estimating seismic attenuation (Q) from VSP data at a heavy oilfield: Ross Lake, Saskatchewan: CREWES Research Report, 16.
Taner, M. T., et al, 1979, Complex seismic trace analysis: Geophysics, 44, 1041-1063.
Tonn, R., 1991, The determination of the seismic quality factor Q from VSP data: A comparison of different computational methods: Geophysical Prospecting, 39, 1-27.
Udias, A., 1999, Principles of seismology: Cambridge University Press